polarization and kinetic data arise mainly from the different cathodic reactions involved.

A model for thermal oxide growth at ≤ 1 μm in thickness is proposed, based on the kinetic and polarization data.

1. When oxidizing in steam, the reduction of the protons released is assisted by their surface conduction in the adsorbed water phase on the zirconia surface and the electron transport at the intermetallic sites. Therefore, the rest potential stays at low negative values and the oxidation proceeds at a fast rate comparable to that in the molten salts.

2. In dry air, the oxidation proceeds at a much slower rate than in steam and the molten salts. The electrical conduction properties of the oxides grown in air, however, are similar to those of the oxides grown in the molten salts. Therefore, the low rates of oxidation in air are attributed to a highly negative rest potential on the alloy brought about by a high resistance for the surface conduction of electrons and the absence of a reduction step involving cationic species. The rate of oxidation, initially linear, is controlled by the reduction of oxygen at the surface; then the rate changes due to the buildup of an electronic space charge in the oxide and control by the combination of electron conductivity at the intermetallics and surface conduction.

Acknowledgments

The author wishes to acknowledge the many helpful discussions he had with Dr. B. Cox and the assistance offered by Mr. V. C. Ling in sample preparation.

Manuscript submitted Jan. 5, 1980; revised manuscript received May 20, 1980. This was Paper 63 presented at the Seattle, Washington, Meeting of the Society, May 21-26, 1978.

Any discussion of this paper will appear in a Discussion Section to be published in the December 1981 JOURNAL. All discussions for the December 1981 Discussion Section should be submitted by Aug. 1, 1981.

Publication costs of this article were assisted by Atomic Energy of Canada Limited.

REFERENCES

1. A. L. Bacarella and A. L. Sutton, *This Journal*, **112**, 546 (1965).
2. M. L. Brown and G. N. Walton, *J. Nucl. Mater.*, **66**, 44 (1977).
3. D. H. Bradhurst, J. E. Draley, and C. J. Van Drunen, *This Journal*, **112**, 1171 (1965).
4. J. H. Eriksen and K. Hauffe, *Z. Phys. Chem. N.F.*, **59**, 332 (1968).
5. B. Cox, *J. Nucl. Mater.*, **31**, 48 (1969).
6. N. Ramasubramanian, *ibid.*, **55**, 134 (1975).
7. N. Ramasubramanian, *This Journal*, **127**, 2566 (1980).
8. A. W. Urquhart, D. A. Vermilyea, and W. A. Rocco, *ibid.*, **125**, 199 (1978).
9. B. Cox, in "Advances in Corrosion Science and Technology," Vol. 5, M. G. Fontana and R. W. Staehle, Editors, pp. 301-311 and 343-361, Plenum Press, New York (1976).
10. G. C. Pimentel and A. L. McClellan, "The Hydrogen Bond," p. 31 and 253, W. H. Freeman and Company, San Francisco, California (1960).
11. J. K. Dawson, U. C. Baugh, and J. F. White, in "Zirconium and Its Alloys," J. P. Pemsler, E. C. W. Perryman, and W. W. Smeltzer, Editors, p. 137, The Electrochemical Society Softbound Proceedings Series, New York (1966).

High Oxygen Ion Conduction in Sintered Oxides of the Bi_2O_3-Dy_2O_3 System

M. J. Verkerk and A. J. Burggraaf

Department of Inorganic Materials Science, Twente University of Technology, 7500 AE Enschede, The Netherlands

ABSTRACT

The phase diagram of the Bi_2O_3-Dy_2O_3 system was investigated. A monophasic fcc structure was stabilized for samples containing 28.5-50.0 mole percent (m/o) Dy_2O_3. Above and below this concentration range polyphasic regions appear. The fcc phase showed high oxygen ion conduction. The ionic transference number is equal to one for specimens containing 28.5-40.0 m/o Dy_2O_3, whereas an electronic component is introduced at low temperatures for specimens containing 50.0 m/o Dy_2O_3. The conductivity of $(Bi_2O_3)_{0.715}(Dy_2O_3)_{0.285}$ is 0.71 $\Omega^{-1}m^{-1}$ and 14.4 $\Omega^{-1}m^{-1}$ at 773 and 973 K, respectively. Relations were found between the ionic radius, the conductivity, and the minimum concentration of lanthanide necessary to stabilize the fcc phase. It is concluded that the highest ionic conductivity will be found in the system Bi_2O_3-Er_2O_3 or Bi_2O_3-Tm_2O_3. From a study of relations between the activation energy, log σ_0 and the composition it is concluded that two conductivity mechanisms play a role.

Recently Harwig investigated the electrical and structural properties of Bi_2O_3 (1-5). At room temperature the monoclinic α-phase is stable and the conductivity is predominantly electronic. On heating to 1002 K the oxide transforms to the face centered cubic (fcc) δ-phase, which is stable up to the melting point at 1097 K. In the δ-phase the electrical conductivity is about 100 $\Omega^{-1}m^{-1}$ and varies little with temperature. The ionic transport number is equal to one (6). On cooling this highly conductive phase may be extended to 923 K, where it transforms into the tetragonal β-phase or to 912 K where it transforms into the body-centered cubic (bcc) γ-phase. These phase transformations are accompanied by sudden volume changes which cause deterioration of the mechanical properties of the material. The conductivity in the β- and γ-phase is mainly ionic and about three orders of magnitude lower than in the δ-phase.

The temperature range at which this material can be used as a solid electrolyte can be extended by substituting Bi_2O_3. The region of highly ionic conductive δ-phase can be extended to room temperature by intro-

Key words: ionic conductor, solid electrolyte, bismuth oxide, lanthanide oxide, phase relations.

duction of 17.5-45 m/o Er_2O_3 (7,8), 25-43 m/o Y_2O_3 (9), 35-50 m/o Gd_2O_3 (10), 25 m/o WO_3 (11), 15-25 m/o Nb_2O_5 and 18-25 m/o Ta_2O_5 (12). The highest ionic conductivity is found in the system Bi_2O_3-Er_2O_3. The conductivity of $[Bi_2O_3]_{0.80}(Er_2O_3)_{0.20}$ is 2.3 and 37 $\Omega^{-1}m^{-1}$ at 773 and 973 K, respectively (7).

Oxygen ion conductors based on bismuth sesquioxide are substantially more conductive than the stabilized zirconias. In the temperature range 773-973 K the conductivity of $(Bi_2O_3)_{0.80}(Er_2O_3)_{0.20}$ is about 50-100 times higher than the conductivity of $(ZrO_2)_{0.915}(Y_2O_3)_{0.085}$.

Because of the relative ease of reduction at higher temperatures (6, 13, 14), the bismuth sesquioxide-based materials are not suitable for fuel cell applications. Their application will be limited to oxygen pumps [*e.g.*, for oxygen-enrichment (15)] or electrolyte for "second generation" oxygen sensors [*e.g.*, the device developed by Heyne (16, 17)]. The "second generation" oxygen sensor is used for automotive control and operates in the lean air/fuel ratio region, *e.g.*, an oxygen-rich exhaust gas (1-10% O_2). The sensor produces a feedback signal to keep the gas mixture fed to the motor oxygen rich. So all the fuel is burned and most pollutants can be removed catalytically (16, 18, 19).

The occurrence of the cubic phase (fcc) in the Bi_2O_3-Dy_2O_3 system is reported for $3Bi_2O_3 \cdot Dy_2O_3$ by Datta and Meehan (20) and for $Bi_2O_3 \cdot Dy_2O_3$ by Nasanova *et al.* (21). The fcc phase in comparable binary compounds exhibits high oxygen ion conduction over a wide temperature range. Therefore, the authors have investigated the phase diagram and the conductivity of the Bi_2O_3-Dy_2O_3 system.

The investigations are a part of our studies on a number of Bi_2O_3-Ln_2O_3 compositions. Phenomenological relations between the ionic radius of the lanthanide, the structure, and the conductivity are given. Some predictions about high ionic conductivity in stabilized Bi_2O_3 are made.

Experimental

Preparation and analysis of the specimens.—Bi_2O_3 (Merck, very pure) and Dy_2O_3 (Serva, 99.9%) were thoroughly mixed and prefired at 1020-1120 K for 16 hr, finely ground and isostatically pressed at about 400 MPa, sintered in air for 45 hr, and cooled down (1/2 K min^{-1}) to room temperature. The sintering temperature was raised as the content of Dy_2O_3 was increased, see Table I. Prefiring and sintering were performed in platinum crucibles.

After the synthesis the composition of the samples was checked with x-ray fluorescense. The accuracy is 0.1% absolute. The specimens were analyzed for small amounts of aluminum and silicon. The procedure is described elsewhere (7, 22). The detection limits of these analyses are 0.005 weight percent (w/o) Al and 0.001 w/o Si.

The crystal structures of the specimens were identified by a Philips PW 1370 diffractometer. Cu Kα radiation was used with a Ni filter. The lattice parameters were calculated from diffraction angles in the 60°-120° (2θ) region, obtained at a scanning speed of 1/4° min^{-1} using $Pb(NO_3)_2$ as the internal standard. High temperature x-ray experiments were performed with a Guinier-Simon camera (heating rate: 5 K hr^{-1}). The ceramic structures of polished and thermally etched samples were investigated with the scanning electron microscope (SEM) Type JEOL JSM U3. Differential thermal analysis (DTA) measurements were performed with a du Pont 990 Thermal Analyser, heating rate: 10 or 15 K min^{-1}. The densities of the samples were measured at 298 K by the Archimedes method using mercury.

Measurement of the ionic conductivity.—The electrical conductivity was measured at a frequency of 10 kHz. The ionic transference number was measured by the emf of an oxygen gas concentration cell. Details of these measurements are described elsewhere (7).

Table I. Sintering temperature and density

x in $(Bi_2O_3)_{1-x}(Dy_2O_3)_x$	Temperature (K)	Density* (%)
0.05-0.10	1073	
0.15-0.25	1173	
0.28-0.35	1273	92
0.40-0.50	1373	94
0.60	1373	

* Density is given as a percentage of the theoretical density based on defect fluorite-type lattice.

Results

Samples prepared.—The densities of the specimens after sintering were 92-94% of the theoretical density, see Table I. The avrag grain size of the samples is about 30 μm. The ceramic structure of a specimen is shown in Fig. 1. On this photograph it can be seen that the grain growth in this system is very fast even at temperatures of 1273 K. The grain boundaries move so fast that they become curved and pores are isolated within the grains. This implies that higher final densities are difficult to obtain without controlling grain growth.

The color of the specimens was yellow/orange for low percentages of Dy_2O_3 and dark brown for high percentages.

The difference between the calculated composition and the composition measured by x-ray fluorescence was 2.0% absolute or less. Concentrations of silicon and aluminum impurities are lower than 0.002 and 0.03 w/o, respectively.

Structural aspects.—Table II gives a survey of the existing structures if the specimens are subjected to different heat-treatments. In the "quenching" procedure the samples were suddenly removed from the furnace and cooled down to room temperature by natural convection, with the result that the high temperature structure could be retained. Lower temperature phases are occasionally achieved by cooling down very slowly (1/2 K min^{-1}) or by annealing at a suitable temperature.

The sample containing 5 m/o Dy_2O_3 has a tetragonal structure. The high temperature structure is cubic (fcc) as determined by the High Temperature Guinier technique (HTG). The transition temperature is 913 K, see Table III. If this sample is annealed, minor concentrations of other phases appear. This was also

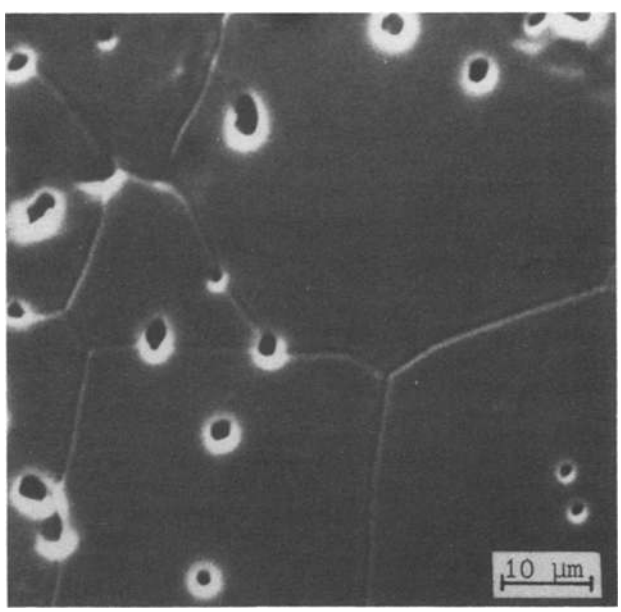

Fig. 1. The ceramic microstructure of $(Bi_2O_3)_{0.65}$ $(Dy_2O_3)_{0.35}$

Table II. Survey of the structural information of the Bi_2O_3-Dy_2O_3 system

x in $(Bi_2O_3)_{1-x}(Dy_2O_3)_x$	Temperature treatment: "Quenched" at sintering temperature	Cooled down by ½ K min^{-1}	Annealing temperature (K)	Annealed for 350 hr
0.05	β*	β	823	$\beta + \underline{\alpha} + \underline{\epsilon}$
0.10	δ	$\delta + \underline{\epsilon}$†,‡	823	$\alpha + \delta + \epsilon$
0.15	δ	$\epsilon + \underline{\delta}$	903	$\epsilon + \underline{\alpha}$
0.20	δ	$\epsilon + \underline{\delta}$	973	$\epsilon + \underline{\delta}$
0.25	δ	δ	973	$\epsilon + \underline{\delta}$
0.28[5]-0.50	δ	δ	973	δ
0.60	$\delta + \theta$**	$\delta + \theta$		

* The β-phase has a tetragonal structure.
** In this table θ denotes the unknown structure.
† In this table ϵ denotes the rhombohedral structure.
‡ The underlined structures appear in minor concentrations.

observed in the Bi_2O_3-Er_2O_3 system (7). Possibly the tetragonal solid solution phase is stable at higher temperatures (*i.e.*, between 823-913 K) whereas at lower temperatures the solid solution exists over a narrower range of composition and ultimately only one tetragonal compound exists. It is suggested that this is the case in the Bi_2O_3-Y_2O_3 system (20).

The high temperature structure of the sample containing 10-25 m/o Dy_2O_3 is cubic (fcc). This can be concluded from the quenching experiments and was checked by HTG. The low temperature structure is rhombohedral, as can be seen from the samples cooled down by 1/2 K min^{-1} as well as from the annealing experiments. The annealing experiments indicate that the rhombohedral solid solution is found from about 15 m/o Dy_2O_3 to 25 m/o Dy_2O_3. After annealing for 2000 hr at 880 K the structure of the specimen containing 25 m/o Dy_2O_3 was $\geq$ 95% rhombohedral. Table III shows the transition temperature of the rhombohedral structure to the cubic structure measured by DTA.

The equilibrium monophasic fcc structure was observed at low temperatures for samples containing 28.5-50.0 m/o Dy_2O_3. These results do not agree with the observations of Datta and Meehan (20) who reported the existence of the fcc phase for $3Bi_2O_3 \cdot Dy_2O_3$ at low temperatures. It is very likely that these authors reported the nonequilibrium high temperature structure. Possibly contamination by the porcelain or silica crucibles used for the synthesis of the materials may play a role. The observations of the fcc phase for $Bi_2O_3 \cdot Dy_2O_3$ by Nasonova *et al.* (21) is confirmed.

As shown in Fig. 2 we see that in the whole range of the stabilized fcc phase (28.5-50 m/o Dy_2O_3) and in the range where the high temperature fcc phase can be retained by quenching (10-25 m/o Dy_2O_3) the lattice constant decreases linearly with an increasing Dy_2O_3 content, *i.e.*, Vegard's rule holds.

The specimen containing 60 m/o Dy_2O_3 shows an fcc phase and an unknown phase. Attempts to determine the composition of the two phases with the EDAX unit of the SEM failed because the size of the separate phases was too small compared to that of the analyzed area (0.5-1 μm^2). The deviation of the lattice constant of the fcc phase, see Fig. 2, cannot be explained.

Table III. Transition temperatures measured by DTA in the heating-up direction*

x in $(Bi_2O_3)_{1-x}(Dy_2O_3)_x$	Transition	Temperature (K)
0.05	$\beta \rightarrow \epsilon$	913
0.10	$\epsilon \rightarrow \delta$	848
0.15	$\epsilon \rightarrow \delta$	946
0.20	$\epsilon \rightarrow \delta$	989
0.25†	$\epsilon \rightarrow \delta$	1018

* Measured on samples cooled down by ½ K min^{-1} from sintering temperature.
† Measured on the annealed sample (2000 hr at 880 K).

The theoretical densities can be calculated from the measured lattice constants assuming several defect models and can be compared with the observed densities. These defect models are extensively described and discussed in Ref. (7) and will not be repeated here. It appears that the system Bi_2O_3-Dy_2O_3 shows the same features as reported for Bi_2O_3-Er_2O_3 (7). So we conclude that all cations occupy their normal sites in the fluorite structure and that there are two vacancies in a unit cell, *i.e.*

$$Bi_{4(1-x)}Dy_{4x}O_6\square_2$$

Conductivity of the sintered specimens.—The conductivity of the sintered Bi_2O_3-Dy_2O_3 samples measured in air is shown in Fig. 3 and 4. In Fig. 4 the conductivity of pure Bi_2O_3 [after Takahashi *et al.* (6)] is given as a reference material. Table IV summarizes the values of the activation energies E_a and the preexponential terms σ_0 for the Arrhenius plots of the conductivity, while the deviation is given in the 90% reliability interval.

Figure 3 gives the conductivity of the cubic and rhombohedral structures of $(Bi_2O_3)_{0.75}(Dy_2O_3)_{0.25}$. Below 1018 K the cubic phase is unstable but can exist metastable because the transformation is too slow in order to take place during the rapidly performed conductivity measurements, see Table II. For the rhombohedral specimen these is a change in the activation energy at about 780 K. Possibly this may be correlated with a change in the ordering of oxygen in the lattice, as proposed for the cubic samples (see below). At 1010 ± 15 K there is a sudden increase in the conductivity. According to the HTG experiments this increase is caused by the structural change from the rhombohedral to fcc phase. The transformation temperature corresponds with the DTA data, see Table III. In the Arrhenius plot of the cubic sample

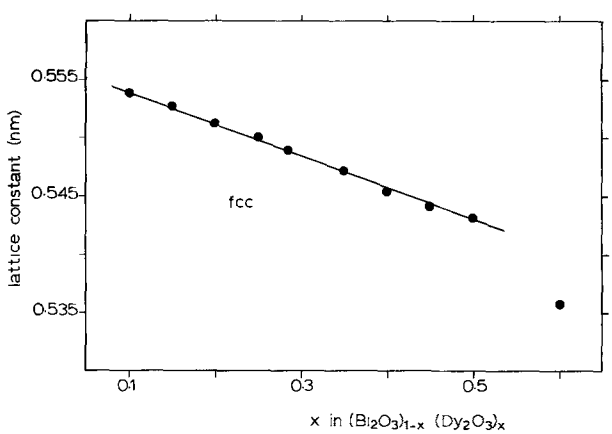

Fig. 2. Lattice constant of the fcc phase of the specimens cooled from the sintering temperature to room temperature by 1/2 K min^{-1}. (For $x = 0.1$-0.2 the specimens were quenched.)

Table IV. Activation energies and pre-exponential terms for the Arrhenius plots of the conductivity

x in $(Bi_2O_3)_{1-x}(Dy_2O_3)_x$	Temperature range (K)	log σ_0 ($\Omega^{-1}m^{-1}$)	E_a (kj mole^{-1})
0.25 (rhom)	600-780	5.3 ± 0.2	97 ± 3
	780-1000	4.4 ± 0.1	85 ± 2
0.25 (cubic)	600-870	7.2 ± 0.2	104 ± 3
	870-1060	5.0 ± 0.2	66 ± 4
0.28[5]	600-870	7.17 ± 0.04	108 ± 1
	870-1140	5.1 ± 0.1	73 ± 3
0.35	600-950	6.33 ± 0.05	101 ± 1
	950-1140	4.8 ± 0.1	73 ± 2
0.40	600-1050	6.34 ± 0.06	107 ± 1
0.45	600-1050	6.4 ± 0.4	112 ± 6
0.50	600-1050	5.9 ± 0.1	109 ± 2
0.60	600-1050	5.1 ± 0.1	112 ± 2

there is a change in the activation energy at about 870 K, this is discussed below.

The structure and the dimensions of the lattices of these phases are very different and the influence on the conductivity is striking. The volume of the rhombohedral and cubic unit cells is 0.123 and 0.166 nm^3, respectively. The cubic lattice is "blown up" compared with the rhombohedral one. Therefore a flat potential profile along the transport path between oxygen ion lattice sites can be expected and rapid transport can occur in the cubic lattice, as suggested for other systems by Huggins (23).

Figure 4 gives the Arrhenius plots of the conductivity of the cubic specimens containing 0.25-0.60 m/o Dy_2O_3. The samples containing 0.25-0.35 m/o Dy_2O_3 show a knee in the Arrhenius plot at about 870-950 K. The changes in the activation energies and the pre-exponential terms are given in Table IV. Present authors (7) correlated this knee to a change in the lattice constant, probably caused by changes in the ordering of oxygen in the lattice. The increase of the lattice constant for $(Bi_2O_3)_{0.80}(Er_2O_3)_{0.20}$ was confirmed by the Simon camera and is in the order of 1.5%. However, for the samples containing Dy_2O_3 no increase in the lattice constant could be measured with HTG. We conclude that the change in activation energy and the change in log σ_0 is caused by a minor change in the structure which is not always accompanied by a measurable change in the unit cell volume.

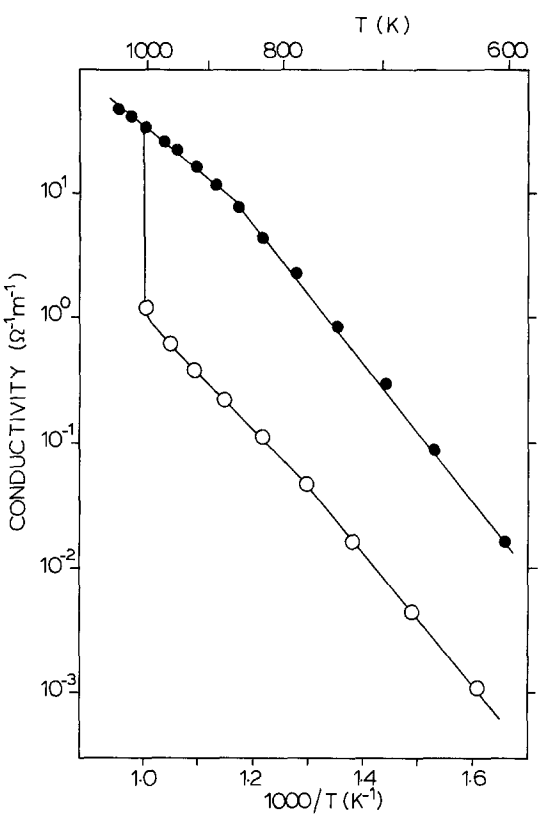

Fig. 3. Conductivity of $(Bi_2O_3)_{0.75}$ $(Dy_2O_3)_{0.25}$ in air. ●, Cubic structure; ○, rhombohedral structure. The specimen with the rhombohedral structure could only be measured in the heating-up direction (see text).

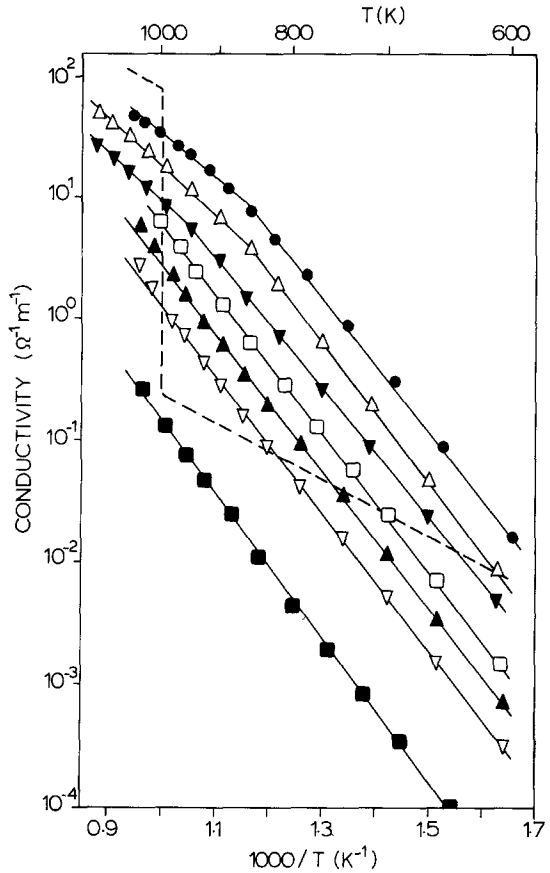

Fig. 4. Conductivity of $(Bi_2O_3)_{1-x}$ $(Dy_2O_3)_x$ in air. ●, x = 0.25 (fcc); △, x = 0.28[5]; ▼, x = 0.35; □, x = 0.40; ▲, x = 0.45; ▽, x = 0.50; ■, x = 0.60. The broken line represents the conductivity of pure Bi_2O_3 in the heating-up direction.

The best oxygen ionic conductor in this system is found in the material with the composition $(Bi_2O_3)_{0.715}(Dy_2O_3)_{0.285}$. The conductivity at 773 and 973 K is 0.71 and 14.4 $\Omega^{-1}m^{-1}$, respectively. This is about three times lower than the conductivity of $(Bi_2O_3)_{0.80}(Er_2O_3)_{0.20}$ (7) and more than ten times higher than the conductivity of $(ZrO_2)_{0.195}(Y_2O_3)_{0.085}$ at the same temperatures.

The ionic transference number.—The ionic transference number was measured with an oxygen gas concentration cell under the condition of P'_{O_2} = 0.21 atm and P''_{O_2} = 1.00 atm. The ratio of the measured emf to the theoretical emf is given in Table V.

For $(Bi_2O_3)_{1-x}(Dy_2O_3)_x$ with x = 0.25-0.40 the ionic transference number is approximately one, therefore the conductivity in the range 1-100% O_2 can be almost wholly attributed to oxygen ions [this work, (27), (31)]. It may be remembered that the deviation of

Table V. Ratios of the measured emf E to the theoretical value E_0 of the following cell:

O_2 (0.21 atm), Pt | $(Bi_2O_3)_{1-x}(Dy_2O_3)_x$ | Pt, O_2 (1 atm) at different temperatures

x in $(Bi_2O_3)_{1-x}(Dy_2O_3)_x$	E/E_0 823 K	873 K	923 K	973 K	1023 K	1073 K
0.25	—	0.93	0.96	0.97	0.98	0.98
0.28[5]	0.94	1.00	0.98	0.98	0.98	0.98
0.40	0.95	0.97	0.99	1.00	1.01	1.00
0.50	—	0.85	0.99	0.94	0.95	0.95
0.60	0.42	0.47	0.54	0.61	0.69	0.72

the ionic transference number measured by oxygen concentration cells is about 5%. Additional experiments are necessary to determine the (small) contribution of the electronic conductivity. The sample containing 50 m/o Dy_2O_3 had an electronic component at low temperatures ($T < 900$ K). For the sample containing 60 m/o Dy_2O_3 an electronic component was measured for all temperatures. Because the ionic transference number for the monophasic fcc samples coexisting with the second phase is approximately one, the electrical conductivity has to be ascribed to the second phase. In this temperature range and at these oxygen partial pressures pure Dy_2O_3 is an electronic conductor (24). Possibly the unknown phase is Dy_2O_3 rich.

Discussion

The results of this study were combined with literature data of the following systems: Bi_2O_3-Er_2O_3 (7, 8), Bi_2O_3-Y_2O_3 (9), Bi_2O_3-Gd_2O_3 (10), and Bi_2O_3-Yb_2O_3 (25). Our attention is directed to two subjects, first, the optimalization of the conductivity in sintered oxides of the Bi_2O_3-Ln_2O_3 system and, second, some considerations concerning the defect structure.

The optimalization of the conductivity.—The conditions leading to an optimal conductivity of sintered oxides of the Bi_2O_3-Ln_2O_3 system were investigated concerning several aspects. These are, first, the influence of the ionic radius on the conductivity, second, the influence of the composition on the conductivity, and third, the influence of the ionic radius on the minimum substituent concentration necessary to stabilize the fcc phase.

Figure 5 gives the conductivity of bismuth sesquioxide stabilized by several lanthanides as a function of the ionic radius of the substituent. The ionic radii are based on $r(^{VI}O^{2-}) = 0.140$ nm, coordination number VIII, as given by Shannon and Prewitt (26). The conductivity increases slightly with increasing ionic radius. No precise data about the lattice constants for some of the compositions are known. However, there is a linear relation between the ionic radius of the substituent and the lattice constant, as shown by Cahen (27), and thus there is a linear relation between the conductivity and the lattice constant. There is too little precise data known up till now to analyze this relation further in terms of relationships between the lattice constant and log σ_0 respectively E_a.

We propose that it may be ascribed to a change in E_a. Assuming the same defect structure for all substituents at $x = 0.35$ the amount of vacancies is constant, so log σ_0 will also be constant. Increasing the ionic radius of the substituent will cause an increase in the lattice constant. This may cause a decrease in the contributions of the local strain components during the passage of oxygen ions through the lattice, which leads to a decrease in the activation energy. This explanation agrees with the observation that the slope of the log σ *vs.* r_{ion} relation at 773 K is larger than that at 973 K. This hypothesis is confirmed in a related system. Kubo and Obayashi (28) showed that in $Ce_{1-x}Ln_xO_{2-x/2}$ for $x = 0.30$ the activation energy decreases with increasing ionic radius of the lanthanide.

In Fig. 6 the oxygen ion conductivity in the Bi_2O_3-Dy_2O_3 system is plotted against the Dy_2O_3 content at different temperatures. The conductivity of $(Bi_2O_3)_{0.80}(Er_2O_3)_{0.20}$ (7) is given as a reference. In the fcc solid solution phase field the conductivity decreases linearly with the composition. For $x = 0.60$ there is a negative deviation from this linear relation. This is due to the second phase. The deviation at $x = 0.25$ is caused by a structural phase transformation. The conductivity of the metastable fcc phase at $x = 0.25$ satisfies this linear relation as shown in Fig. 6. It should be noted that a linear relation between conductivity and concentration holds at temperatures above and below the observed knee in the Arrhenious plot. A linear relation in the fcc solid solution phase field is also found for Bi_2O_3 stabilized with Er_2O_3 (7), Y_2O_3 (9), and Gd_2O_3 (10).

From the Fig. 5 and 6 it is clear that the highest ionic conductivity will be found for large ions and low substituent percentages. As will be shown, these are contradictory requirements. Attention should be paid to the influence of the ionic radius of the Ln^{3+} ion on the minimum substituent concentration ($x_{min.}$) necessary to stabilize the fcc structure at room temperature. The correlation between the ionic radius and $x_{min.}$ is given in Fig. 7. It should be noted that the minimum concentrations given in (9, 10) for Gd_2O_3 and Y_2O_3 may be too low. Present work and (7) show that high temperature structures may be easily retained at low temperatures. So the cooling procedures applied in (9, 10) to determine the phase boundary of the fcc structure may not be sufficient to produce the "equilibrium" phase boundary. Figure 7 shows that there is a minimum in this curve at $r_{ion.} = 0.100$ nm (Er^{3+}). In literature there are no data about $x_{min.}$ for Ln = Tm^{3+} ($r_{ion} = 0.009$ nm). So it is possible that $x_{min.}$ for Tm^{3+} is somewhat lower than for Er^{3+}.

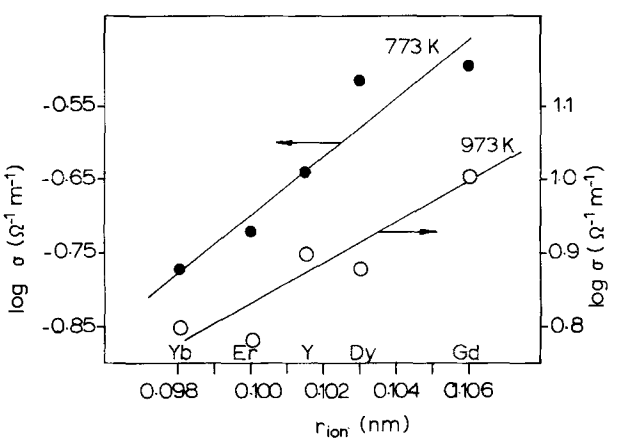

Fig. 5. The logarithm of the conductivity of $(Bi_2O_3)_{0.65}(Ln_2O_3)_{0.35}$ vs. the ionic radius of the substituent Li^{3+} at 737 K (closed circles) and at 973 K (open circles).

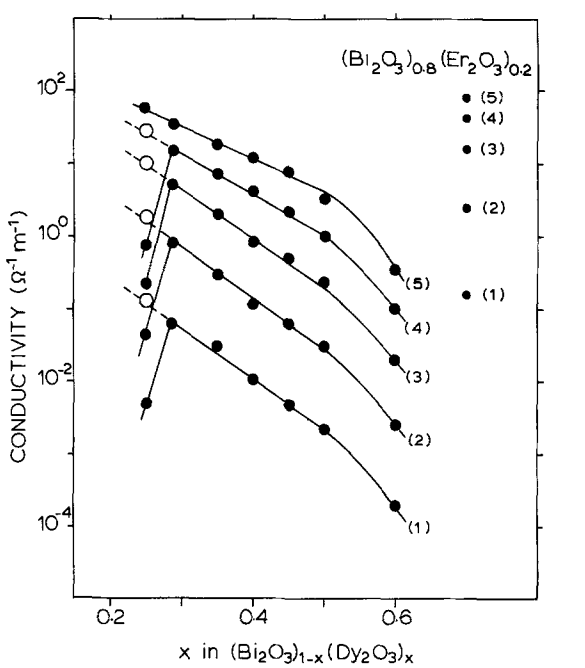

Fig. 6. Conductivity vs. composition at different temperatures. At the right the conductivity of $(Bi_2O_3)_{0.80}(Er_2O_3)_{0.20}$ is given as a reference. Curve 1, 673 K; curve 2, 773 K; curve 3, 873 K; curve 4, 973 K; curve 5, 1073 K. (The open circles represent the conductivity of the metastable fcc phase.)

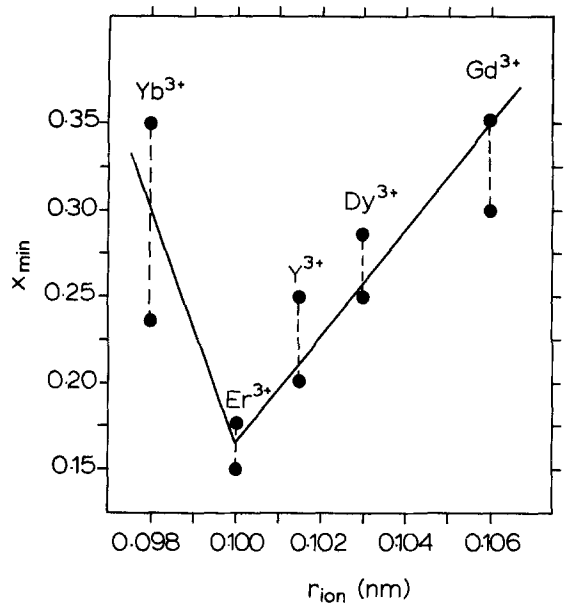

Fig. 7. X_{min} vs. the ionic radius (r_{ion}) of the substituent

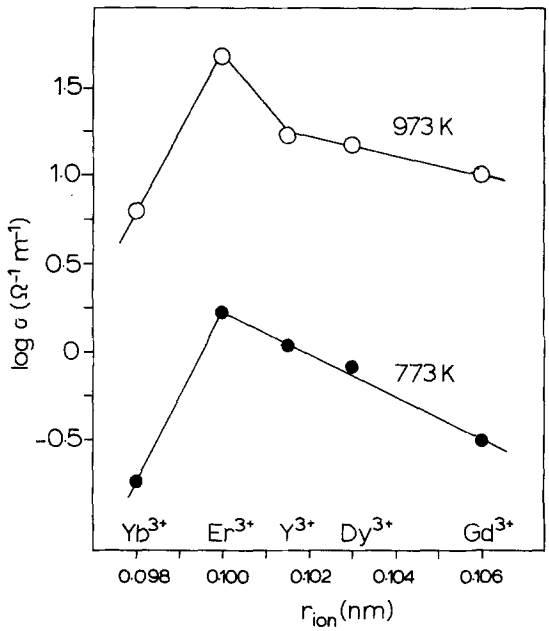

Fig. 8. The conductivity of $(Bi_2O_3)_{1-x}(Ln_2O_3)_x$ for x is the upper boundary of $X_{min.}$ vs. the ionic radius of the substituted Ln^{3+} at 737 K (closed circles) and at 973 K (open circles).

The shape of the curve may be qualitatively explained in the following way. We assume that stabilization of the (very open) high temperature structure occurs at a certain contraction of this structure by the substituent. If the difference between the ionic radii of Bi^{3+} (0.111 nm) and the substituted M^{3+} is large, this will result in a large distortion in the host lattice and a small amount of substituent is necessary for supplying the energy required to stabilize the fcc phase, *i.e.*, for Er^{3+}. Reversely, a small difference between the ionic radii needs a large amount of substituent to supply the energy to stabilize the fcc phase, *i.e.*, for Gd^{3+}. For too large differences between the ionic radii of the Ln^{3+} ion and the Bi^{3+} ion the fcc phase becomes disfavored. At this stage we do not understand the stabilization of the fcc phase at higher concentration of Yb^{3+}, *i.e.*, a substituent with a relatively large difference in ionic radius with respect to Bi^{3+}.

From Fig. 5 we can conclude that the fcc structure will also be stabilized at low temperatures for Ln = Tm (r_{ion} = 0.099 nm), Ln = Ho (r_{ion} = 0.102 nm), Ln = Tb (r_{ion} = 0.104 nm), and possibly for Ln = Sm (r_{ion} = 0.102 nm). The $x_{min.}$ values for these substituents are predicted in this figure.

This discussion allows us to make some predictions about optimalization of the ionic conductivity of Bi_2O_3 stabilized by lanthanides. There are two contradictory tendencies. First, the ionic conductivity increases with increasing ionic radius (Fig. 5). Second, $x_{min.}$ increases with increasing ionic radius (Fig. 7) and a high $x_{min.}$ value results in a low conductivity (Fig. 6). However, the influence of the ionic radius on the conductivity is smaller than the influence of the Ln_2O_3 content. Therefore the optimalization of the conductivity is only possible by lowering $x_{min.}$. Figure 7 shows that there is a minimum in the $x_{min.}$ *vs.* r_{ion} plot at 0.098 nm < r_{ion} < 0.105 nm. The ions Er^{3+} (r_{ion} = 0.100 nm) and Tm^{3+} (r_{ion} = 0.099 nm) fall within this range. The highest conductivity occurs at the lowest $x_{min.}$, as shown in Fig. 8. We conclude that the highest ionic conductivity will be found for Bi_2O_3 stabilized by Er_2O_3 or Tm_2O_3.

If the conductivity above the knee could be stabilized at low temperature, a further optimalization of the conductivity could be achieved. As shown below, the knee is correlated with an ordering process in the oxygen lattice. Therefore it is not very likely that the high temperature conductivity can be stabilized at lower temperatures.

Defect structure.—As pointed out before the knee in the Arrhenius plot cannot simply be ascribed to a change in the lattice constant, but has to be ascribed to a change in the defect structure. At about the same temperature a knee in the Arrhenius plot is reported for Bi_2O_3 stabilized with Er_2O_3 (7), Y_2O_3 (9), and Gd_2O_3 (10), for yttria-stabilized zirconia (29, 30) and for lanthanide-doped ceria (28).

From this work and the results mentioned in literature (7, 9, 10) we searched for relations between the activation energy, log σ_o, and the lanthanide content. For reasons of clarity the data are separately given for temperatures below 820 K and above 900 K. The results are given in Fig. 9 and 10. It appears that there are two different dependences, which can be related to different defect structures.

Above 900 K for the samples showing a knee in the Arrhenius plot the activation energy increases with increasing x whereas log σ_o is independent of x. The values of the activation energy and log σ_o, extrapolated to x = 0, come very close to the values of δ-Bi_2O_3. This suggests a disordered oxygen lattice analog to pure δ-Bi_2O_3 (4).

For the samples showing no knee in the Arrhenius plot, it appears that the activation energy is independent of x and log σ_o decreases linearly with increasing x. The same holds below 820 K for the samples showing a knee in the Arrhenius plot. These relations suggest that in this region the composition and therefore the lattice constant have no significant influence on the thermal activated passage of oxygen ions through the lattice, whereas the composition has a strong influence on log σ_o. The hypothesis is put that in this region the oxygen ions are ordered. The concentration of the mobile oxygen ions strongly decreases with increasing lanthanide content.

This hypothesis is supported by neutron diffraction studies at room temperature by the present authors on $(Bi_2O_3)_{0.80}(Er_2O_3)_{0.20}$ which show a peak in the diffuse background, which can be correlated with a short distance ordering of oxygen ions. Further neutron diffraction studies are now being performed and will be correlated with a detailed description of the conductivity mechanism.

Conclusions

High oxygen ion conduction is found in the system Bi_2O_3-Dy_2O_3. The fcc phase can be stabilized by 28.5-50.0 m/o Dy_2O_3. For the samples containing 28.5-40.0

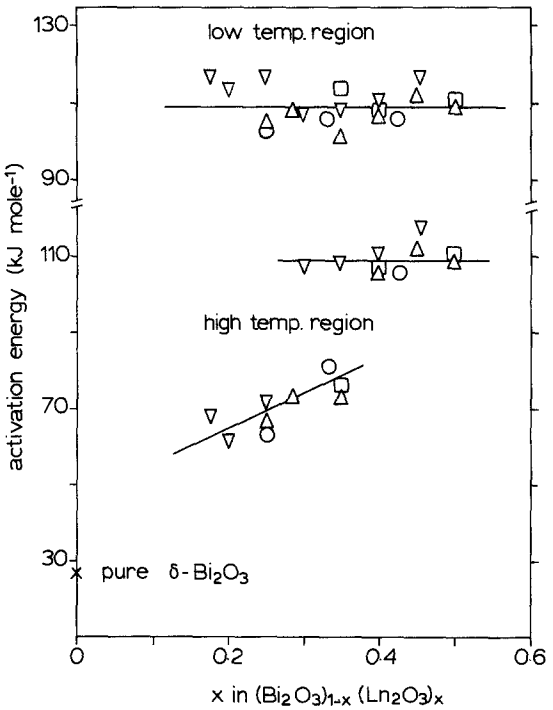

Fig. 9. The activation energy of the conductivity for the low temperature region (<820 K) and for the high temperature region (>900 K) as a function of the composition for several substituents. ○, Ln = Y; □, Ln = Gd; △, Ln = Dy; ▽, Ln = Er.

m/o Dy_2O_3 the ionic transference number is one over the whole temperature range investigated, whereas for the sample containing 50.0 m/o Dy_2O_3 an electronic component is introduced at low temperatures. The conductivity of the most desirable composition in this system, *i.e.*, $(Bi_2O_3)_{0.715}(Dy_2O_3)_{0.285}$, is about three times lower than the conductivity of the best oxygen ion conductor reported for Bi_2O_3-based solid solutions.

It is concluded that the lowest percentage of lanthanide necessary to stabilize the fcc phase is found for Er_2O_3 or Tm_2O_3.

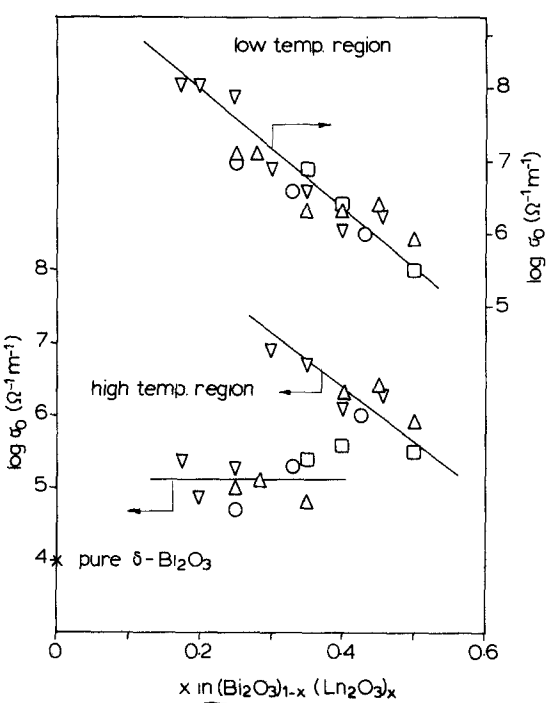

Fig. 10. The log σ_0 of the conductivity for the low temperature region (<820 K) and for the high temperature region (>900 K) as a function of the composition for several substituents. ○, Ln = Y; □, Ln = Gd; △, Ln = Dy; ▽, Ln = Er.

The influence of the ionic radius on the conductivity is smaller than the influence of the lanthanide content. Therefore it is concluded that the highest ionic conductivity based on Bi_2O_3 will be found in the systems Bi_2O_5-Er_2O_3 or Bi_2O_3-Tm_2O_3. The knee in the Arrhenius plot of the conductivity of several specimens is ascribed to a charge in the defect structure.

Acknowledgments

Dr. K. Keizer is thanked for performing some preliminary experiments in this system. We would like to express our appreciation to Mrs. A. van Pelt, Mr. J. Boeysma, and Mr. Th. van Dam for their experimental assistance. Financial assistance from Philips N.V. (Elcoma) is gratefully acknowledged.

Manuscript submitted March 4, 1980; revised manuscript received Aug. 7, 1980.

Any discussion of this paper will appear in a Discussion Section to be published in the December 1981 JOURNAL. All discussions for the December 1981 Discussion Section should be submitted by Aug. 1, 1980.

Publication costs of this article were assisted by the Twente University of Technology.

REFERENCES

1. H. A. Harwig, Thesis, State University Utrecht (1977).
2. H. A. Harwig and A. G. Gerards, *Thermochim. Acta*, **28**, 121 (1979).
3. H. A. Harwig and A. G. Gerards, *J. Solid State Chem.*, **26**, 265 (1978).
4. H. A. Harwig, *Z. Anorg. Allg. Chem.*, **444**, 151 (1978).
5. H. A. Harwig and J. W. Weenk, *ibid.*, **444**, 167 (1978).
6. T. Takahashi, H. Iwahara, and Y. Nagai, *J. Appl. Electrochem.*, **2**, 97 (1972).
7. M. J. Verkerk, K. Keizer, and A. J. Burggraaf, *ibid.*, **10**, 81 (1980).
8. K. Keizer, M. J. Verkerk, and A. J. Burggraaf, *Ceramurgia Int.*, **5**, 143 (1979).
9. T. Takahashi, H. Iwahara, and T. Arao, *J. Appl. Electrochem.*, **5**, 187 (1975).
10. T. Takahashi, T. Esaka, and H. Iwahara, *ibid.*, **5**, 197 (1975).
11. T. Takahashi and H. Iwahara, *ibid.*, **3**, 65 (1973).
12. T. Takahashi, H. Iwahara, and T. Esaka, *This Journal*, **124**, 1563 (1977).
13. T. Takahashi, T. Esaka, and H. Iwahara, *J. Appl. Electrochem.*, **7**, 299 (1977).
14. M. J. Verkerk and A. J. Burggraaf, Accepted for publication in *J. Appl. Electrochem.*
15. K. W. Browall, Paper 467 presented at The Electrochemical Society Meeting, Seattle, Washington, May 21-26, 1978.
16. L. Heyne, in "Measurement of Oxygen," H. Degn *et al.*, Editors, Elsevier, Amsterdam, Oxford, New York (1976).
17. L. Heyne, N. M. Beekmans, P. J. Poolman, and R. K. Eijnthoven, Dutch Pat. Appl. 7,309,537 (1973).
18. R. L. Klimisch and J. M. Komarmy, in "The Catalytic Chemistry of Nitrogen Oxides," R. L. Klimisch and J. G. Larson, Editors, Plenum Press, New York (1975).
19. R. Zechall and G. Baumann, *Motortechn. Z.*, **34**, 7 (1977).
20. R. K. Datta and J. P. Meehan, *Z. Anorg. Allg. Chem.*, **383**, 328 (1971).
21. S. N. Nazonova, V. V. Serebrennikov, and G. A. Narnov, *Russ. J. Inorg. Chem.*, **18**, 1244 (1973).
22. H. Kruidhof, *Anal. Chim. Acta*, **99**, 193 (1978).
23. R. A. Huggins and A. Rabenau, *Mater. Res. Bull.*, **13**, 1315 (1978).
24. V. B. Tare and H. Schmalzried, *Z. Phys. Chem. N.F.*, **43**, 30 (1964).
25. M. J. Verkerk, Unpublished work.
26. R. D. Shannon and C. T. Prewitt, *Acta Crystallogr., Sect. B*, **25**, 925 (1969).
27. H. T. Cahen, Thesis, State University Utrecht

(1980).
28. T. Kudo and H. Obayashi, *This Journal*, **122**, 142 (1975).
29. J. E. Bauerle and J. Hrizo, *J. Phys. Chem. Solids*, **30**, 565 (1969).
30. E. Schouler, Thesis, Grenoble (1979).
31. T. Takahashi, T. Esaka, and H. Iwahara, *J. Appl. Electrochem.*, **7**, 303 (1977).

Diffusion-Limited Charge Transport at Platinum Electrodes on Doped CeO_2

D. Braunshtein, D. S. Tannhauser,* and I. Riess

Department of Physics, Technion, Israel Institute of Technology, Haifa, Israel

ABSTRACT

We have measured the d-c and a-c properties of platinum paste electrodes on samples of the solid electrolyte $(CeO_2)_{0.9}(Gd_2O_3)_{0.1}$ in the temperature range 700°-900°C and the oxygen pressure range $1 \geqq P_{O2} \geqq 10^{-4}$ atm. The d-c measurements showed that the current through the system saturated at a value proportional to the oxygen pressure and that the cathode (the electrode where oxygen enters) limits the current. We explain the limitation by a gas diffusion mechanism, which adds a small term to the dynamic resistance of the sample. The dynamic resistance is mainly determined by the resistivity of the electrolyte together with the current constriction at the triple line gas-electrolyte-electrode. A-C measurements gave impedance plots with the shape of a quarter circle, pointing to a diffusion process. We propose as model that part of the oxygen molecules arriving at the triple line is ionized directly and enters the electrolyte, and a second part diffuses as atoms along the interface electrolyte-electrode before being ionized. This model explains the observed quarter circle as well as the impedances measured for $\omega = 0$ and for $\omega = \infty$.

It is well known that electrode impedance plays an important role in the overall impedance of high temperature fuel cells. A large number of papers treat the subject phenomenologically but only a few try to understand the subject in microscopic detail. Some authors measured d-c properties and proposed a detailed model (1-3), other measured also a-c properties but did not analyze the results microscopically (4-7).

In the present paper we report on d-c and a-c properties of platinum electrodes on gadolinia-doped ceria, combined with scanning electron microscope studies of these electrodes. We then present a detailed model for the processes involved.

Very recently two papers by Wang and Nowick (8, 9) reported on a-c and d-c measurements on the same system. We believe that the differences between the results of their work and ours is due to the structure of the electrodes and we shall come back to this in the discussion.

Sample and Electrode Preparation

The starting material for the electrolyte was prepared by coprecipitation of oxalates of cerium and gadolinium and calcination at 1000°C to obtain $(CeO_2)_{0.9}(Gd_2O_3)_{0.1}$. The powder was then pressed at 2000 bar (2×10^8 Nt/m^2) and sintered at 1700°C for 3 hr.

The shape after sintering was a round cylinder 40 mm long and 11 mm across. Pellet-shaped samples about 1 mm thick were cut with a diamond saw from this cylinder. Some additional samples were prepared directly as pellets and sintered under similar conditions. Platinum electrodes were prepared by spreading a thin layer of platinum paste (Engelhard 6082), heating to 900°C at 100°C/hr, and cooling to room temperature in 1 hr. Scanning electron microscope (SEM) pictures confirm that the heating rate is crucial for the electrode resistance: if the rate is too fast (less than a few hours to 900°C) the platinum tends to form separate islands. This was found to increase the impedance of the sample. Figure 1 shows an SEM picture of a Pt-paste electrode heated slowly; it is seen that the platinum grains are connected and do not form separate islands.

The platinum covered surface S_{Pt} equals about 70% of the visual gross electrode area S_E, which is 0.64 cm^2. The cross section of the sample, S_o, is 1.13 cm^2. The typical width of the interconnected platinum islands in Fig. 1 is 2 μm.

We observed also that the surface condition of the sample influences strongly the two-point resistance of the sample. For electrodes prepared on the surface of sintered pellets (the SEM picture of such a surface is shown in Fig. 2) the two-point resistance was a few hundred ohms at 800°C, much higher than the 2.2Ω calculated from the bulk conductivity with the assumption of ideal electrodes (see below). If the surface of the sample was roughened with sandpaper, the

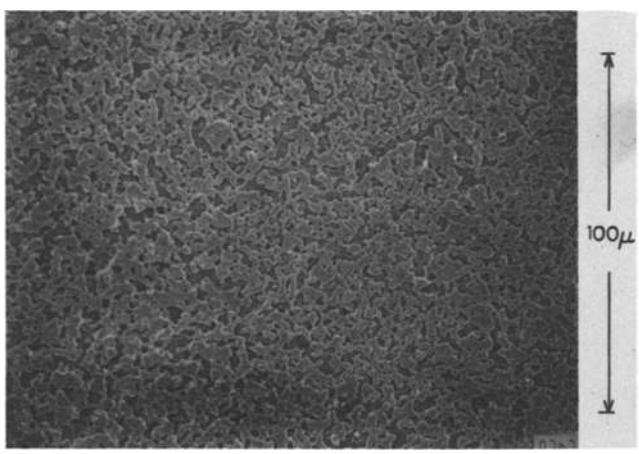

Fig. 1. SEM picture of Pt-paste electrode right after preparation. The lighter areas are platinum.

* Electrochemical Society Active Member.
Key words: fuel cell, solid electrolyte, interface impedance.